IEEE Access
Multidisciplinary ⋮ Rapid Review ⋮ Open Access Journal

Received 5 March 2023, accepted 14 March 2023, date of publication 17 March 2023, date of current version 22 March 2023.

Digital Object Identifier 10.1109/ACCESS.2023.3258701

RESEARCH ARTICLE

High-Precision Measurement of Brillouin Frequency Shift in Brillouin Optical Time-Domain Reflectometer Based on Half-Peak Fitting Algorithm of Power Spectrum

DONG WAN[1,2,3], LINAN SHAN[1,2], LIXIA XI[1,2], ZHENYU XIAO[1,2], YANG'AN ZHANG[1,2], XUEGUANG YUAN[1,2], XIAOSHENG XIAO[1,2], (Senior Member, IEEE), HU ZHANG[1,2], AND XIAOGUANG ZHANG[1,2], (Senior Member, IEEE)

[1]State Key Laboratory of Information Photonics and Optical Communications, Beijing University of Posts and Telecommunications, Beijing 100876, China
[2]School of Electronic Engineering, Beijing University of Posts and Telecommunications, Beijing 100876, China
[3]School of Electronic Information, Beijing Information Technology College, Beijing 100015, China

Corresponding author: Lixia Xi (xilixia@bupt.edu.cn)

This work was supported by the National Natural Science Foundation of China under Grant 62171048, Grant 62071065, and Grant 62075015.

ABSTRACT The Brillouin optical time-domain reflectometer (BOTDR) system, which is based on the Brillouin frequency shift (BFS) of the scattering spectrum, has been widely applied to monitor the temperature and strain in many fields. The measurement accuracy of the BFS directly affects the monitoring and location of the temperature change or strain events. In this study, the characteristics of the least-squares fitting optimal solution of the Brillouin power spectrum are theoretically investigated, and a half-peak fitting algorithm is proposed to measure the BFS with high accuracy and stability. In particular, it can precisely determine the double-peak spectrum and detect the position in the transition section of a temperature change or strain event. Furthermore, it can reduce calculation complexity and enhance measurement speed by dropping most of the data. For the fiber under test (FUT) with a length of 12 km, 200 groups of time-domain data were processed using a probe pulse of width 50 ns and sampling rate 1 GHz. The half-peak fitting algorithm increased the temperature measurement accuracy by ∼1 fold, with ∼20% calculation of full fitting. Meanwhile, it effectively eliminated the influence of minor peak in the double-peak spectrum, and optimized the spatial resolution of the temperature change position to 0.1 m, which is the maximum limitation by sampling rate.

INDEX TERMS Brillouin frequency shift, double-peak fitting, least squares, optical fiber sensors.

I. INTRODUCTION

Brillouin optical time-domain reflectors (BOTDR) are used to realize distributed optical fiber sensing by using the linear relationship of the Brillouin frequency shift (BFS) versus the change in temperature and strain [1]. It has wide applications [2], [3], such as security monitoring of buildings [4], wells [5], marine structures [6], power cables, and traffic facilities [7], [8].

Spectrum analysis based on short-time Fourier transform (STFT) is commonly used in BOTDR systems. It can obtain all the Brillouin scattering spectra in one measurement [9], and its speed is much faster than that of the frequency-scanning method. A smaller STFT window is selected to improve spatial resolution. However, this results in a larger frequency interval. To achieve a high measurement precision, it is important to locate the spectral peak and

The associate editor coordinating the review of this manuscript and approving it for publication was Santosh Kumar.

calculate the BFS based on data from a large interval. Instantaneous frequency analysis can obtain a more accurate BFS [10]; however, it must calculate the instantaneous phase change between two adjacent samples in the time domain, which is complicated and noise sensitive. The curve-fitting algorithm can accurately estimate the peak position. The Lewenberg–Marquardt algorithm used a step factor to reduce dependence on the initial value [11], but it was easily affected by noise. Using the particle swarm optimization algorithm, the fitting outcomes obtained were in good agreement with the real parameters, and the BFS error was reduced [12], [13], whereas the operation time was greatly increased. The artificial neural network model [14] and the wavelet convolutional neural network [15] were suitable to effectively extract the BFS distribution along the fiber, but their calculation complexity and time cost are high.

Another important challenge for curve fitting is that the double-peak Brillouin spectrum occurs over a temperature change or strain event transition section [16], which induces location errors in the BFS measurement. A zero-padded STFT-BOTDR can restore the asymmetric and deforming Brillouin scattering spectrum [17]; however, it caused spectrum leakage and reduces accuracy. A 4th-order Hanning self-convolution window can effectively suppress spectral leakage [18], but the number of calculations required increased significantly. A hybrid optimization algorithm based on shuffled frog leaping and least-squares support vector machine can precisely fit the multipeak spectrum [19]; however, its running efficiency was low.

In this study, a half-peak fitting algorithm based on the least-squares fitting optimal solution of the Brillouin power spectrum was proposed for high-precision measurements. The accuracy and stability of BFS measurements can be increased by selecting the upper half-peak data of the Brillouin power spectrum. Meanwhile, by eliminating the minor peak data, the detection accuracy of the BFS edge was improved, and the spatial resolution of the temperature change or strain event transition section was significantly improved. Furthermore, it reduced computational complexity and increased measurement speed.

II. PRINCIPLE

In BOTDR, the spontaneous acoustic field decays exponentially; therefore, the Brillouin power spectrum naturally broadens to a Lorentzian-curve [20], which can be expressed as Eq. (1):

$$g(v) = g_{\mathrm{p}} \frac{\left(\frac{\Delta v}{2}\right)^2}{(v - v_{\mathrm{B}})^2 + \left(\frac{\Delta v}{2}\right)^2} \tag{1}$$

where $g(v)$ is the Brillouin power spectrum, g_p is the peak power, Δv is the spectrum width, and v_B is the BFS.

According to Eq. (1), the fitting parameters of the Brillouin spectrum can be obtained by least-squares fitting of the power data $(v_1, g(v_1))$, $(v_2, g(v_2))$,..., $(v_n, g(v_n))$, as shown in Eq. (2).

$$g_{\mathrm{p}} = \frac{4C_1}{4C_1C_3 - 2C_2^2},\ v_{\mathrm{B}} = \frac{C_2}{-2C_1},\ \Delta v = \sqrt{4C_3 - \left(\frac{C_2}{C_1}\right)^2} \tag{2}$$

where C_1, C_2, and C_3 are least-squares optimal solutions, as shown in Eq. (3).

$$\begin{bmatrix} C_1 \\ C_2 \\ C_3 \end{bmatrix} = \left(\boldsymbol{V}^{\mathrm{T}}\boldsymbol{V}\right)^{-1}\boldsymbol{V}^{\mathrm{T}}\boldsymbol{G} \tag{3}$$

where

$$\boldsymbol{V} = \begin{bmatrix} v_1^2 & v_1 & 1 \\ v_2^2 & v_2 & 1 \\ \vdots & \vdots & \vdots \\ v_n^2 & v_n & 1 \end{bmatrix},$$

$$\boldsymbol{G} = \begin{bmatrix} \frac{1}{g(v_1)} & \frac{1}{g(v_2)} & \cdots & \frac{1}{g(v_n)} \end{bmatrix}^{\mathrm{T}}.$$

The matrix $\boldsymbol{G}$ of the least-squares optimal solution comprises the reciprocal of the power value. If a value near zero is selected, this will lead to infinity in the matrix $\boldsymbol{G}$, and the fitting will fail because the solution cannot converge. Because the noise spectrum obeys a uniform distribution, the smaller the power, the larger the proportion of noise, and the lower the signal noise ratio (SNR) of power data. According to Eq. (3), the smaller power data with low SNR will induce a larger error of the least-squares optimal solution. Therefore, to successfully fit the Brillouin power spectrum and enhance measurement accuracy, the power data with smaller values should be eliminated in advance.

Moreover, the measurement accuracy depends on the fitting accuracy of the peak in the BOTDR. Therefore, the purpose of the fitting is to locate the peak instead of minimizing the fitting error on the entire curve. As shown in Fig. 1(b), the tail of the power spectrum fluctuates. The better the tail fit, the worse the peak fit. To locate the peak precisely, only data with bigger values and high SNR are selected to be fitted by Lorentzian-curve, and data with smaller values and low SNR are dropped.

The starting and ending frequencies corresponding to the width of the Brillouin power spectrum Δv are $v_1 = v_{\mathrm{B}} - \frac{\Delta v}{2}$ and $v_2 = v_{\mathrm{B}} + \frac{\Delta v}{2}$, and their power is $g(v_1) = g(v_2) = \frac{g_{\mathrm{p}}}{2}$. By calculation, the band energy between v_1 and v_2 is half of the total energy, as shown in Fig. 1(a). Therefore, in the proposed algorithm, $\frac{g_{\mathrm{p}}}{2}$ is used as the threshold to select the data of the power spectrum for curve fitting, as shown in Fig. 1(b). In addition, Using $\frac{g_{\mathrm{p}}}{2}$ instead of a fixed value as the threshold can also weaken the influence of power reduction, which is induced by the dispersion and loss of fiber.

The phonon decay broadens the Brillouin power spectrum, and the half-peak width is $\Delta v = \frac{\Gamma_{\mathrm{B}}}{2\pi}$, where Γ_{B} is the phonon linewidth, which is the reciprocal of phonon lifetime. The phonon lifetime is usually ~10 ns; therefore, the Δv is 10-30 MHz. When the frequency domain width of the STFT

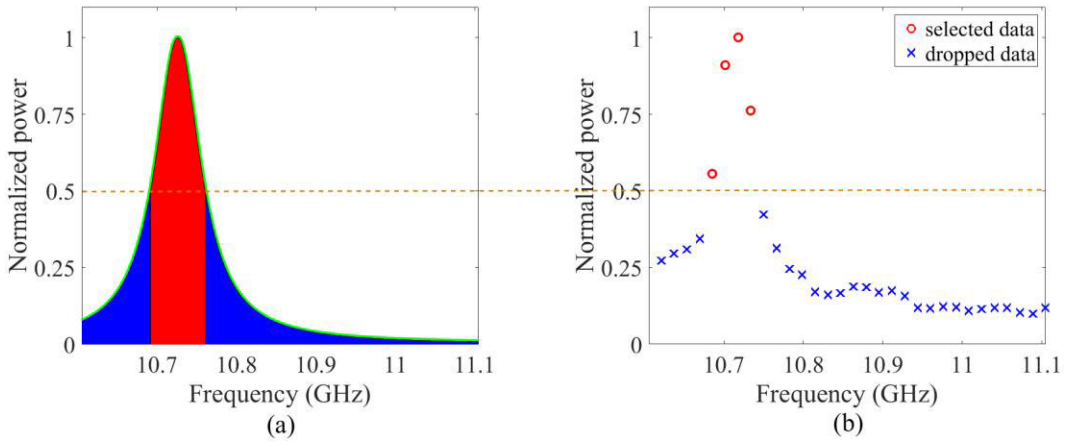

FIGURE 1. Schematic diagram of half-peak data filtering. (a) Lorentzian-curve and (b) data of Brillouin power spectrum.

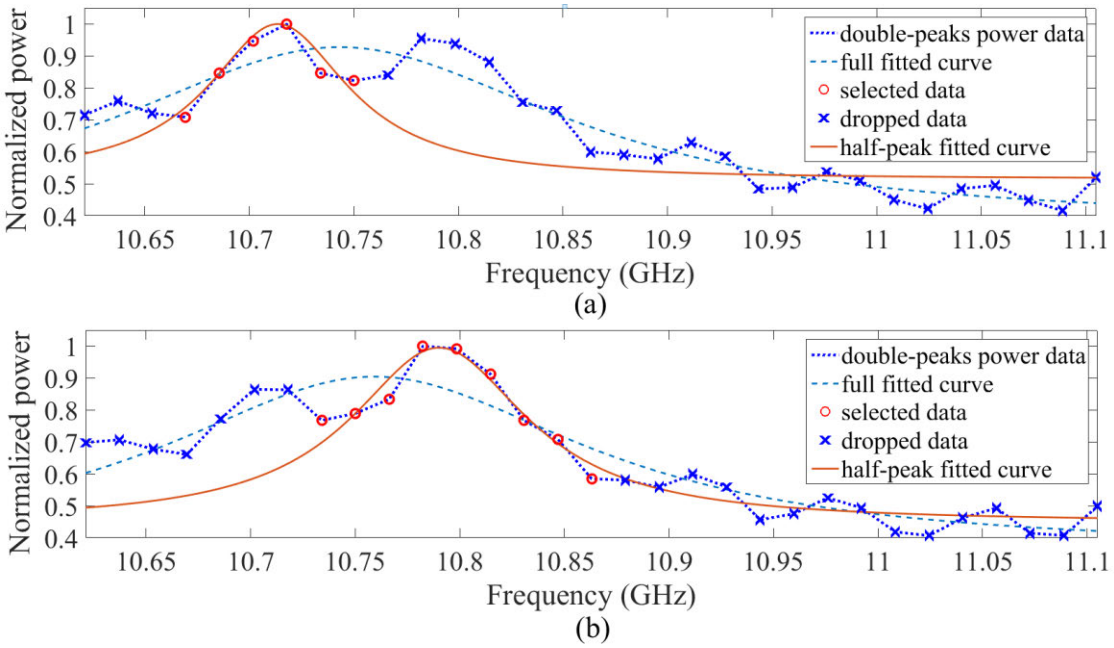

FIGURE 2. Comparison of results between full fitting and half-peak fitting. (a) main peak is on the left and (b) main peak is on the right.

is 100 MHz, the selected data are 10%-30% of the total data. According to Eq. (3), the time complexity of the optimal solution calculation is $O(n)$; therefore, the calculation cost of curve fitting is reduced to 10%-30%.

A double peak exists in the case of a temperature change or strain event transition section in the fiber. If the data of the double-peak spectrum are fully fitted using a Lorentzian-curve, the peak of the fitted curve is located between the two peaks, resulting in a large error in the BFS, as shown in Fig. 2. The proposed half-peak fitting algorithm effectively shields the minor peak data. As shown in Fig. 2(a) and (b), regardless of the side of the minor peak, the main peak data can be selected exactly. The fitted curve is consistent with the shape of a single peak, and the corresponding BFS is accurate. Furthermore, in the case of a temperature change or strain event, the position of the fitting curve jumps; accordingly, BFS also jumps. Combined with a single-step sliding operation, half-peak fitting can determine the location of the event more accurately. More details are presented in Fig. 8 and its descriptions in Section III. Therefore, the proposed algorithm can effectively eliminate the influence of the minor peak and significantly improve the spatial resolution of the temperature change or strain positions.

A flowchart of the proposed half-peak fitting algorithm is shown in Fig. 3. First, the Brillouin scattering signal data were transformed into power spectra using STFT, and the spectra were cumulatively averaged to reduce noise. The data were then selected as follows: find the maximum datum of each power spectrum as the top of the main peak; search towards each side to check whether the datum decreases monotonously and is greater than half of the maximum datum; determine the start and end of the half-peak data; and

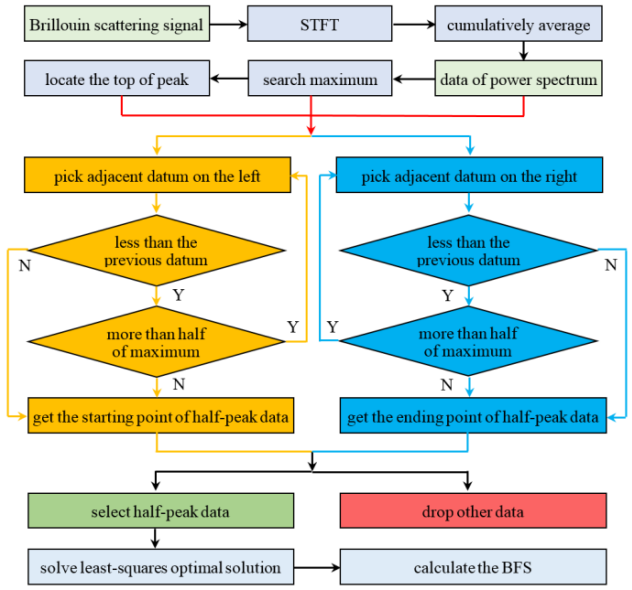

FIGURE 3. Flow chart of half-peak fitting algorithm.

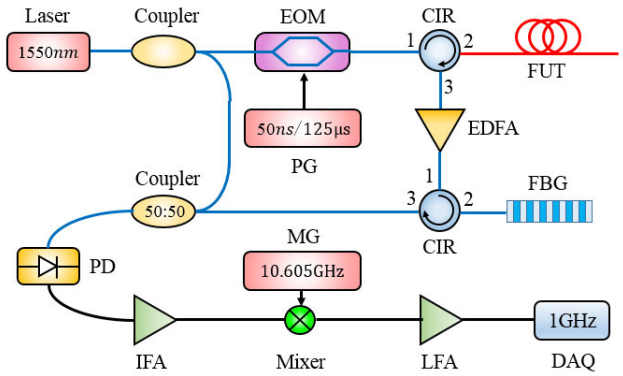

FIGURE 4. Configuration of the BOTDR system. EOM: electro-optic modulator, PG: pulse generator, CIR: circulator, FUT: fiber under test, EDFA: erbium doped fiber amplifier, FBG: fiber Bragg grating, PD: photo detector, IFA: intermediate frequency amplifier, MG: microwave generator, LFA: low frequency amplifier, DAQ: data acquisition card.

select the data between the start and end as the half-peak data. Finally, the half-peak data were substituted into Eq. (3) to calculate the least-squares optimal solutions and obtain the BFS, according to Eq. (2).

It is worth noting that the half-peak fitting algorithm not only selects half-peak data to enhance measurement accuracy but also checks the monotonicity to select the main peak data exactly in the structural geometry of the double-peak profile.

III. EXPERIMENTAL RESULTS AND DISCUSSION

The BOTDR system used in this experiment is illustrated in Fig. 5. The length of the fiber under test (FUT) was 12 km, where a 100 m segment at the 7 km point was heated to 80 °C, while the others were in a room with 20°C temperatures. A light pulse with a 125 *us* period and 50 *ns* width generated by electro-optic modulator (EOM) was injected into the FUT through a circulator to obtain Brillouin scattering signals. The signals were amplified by erbium-doped fiber

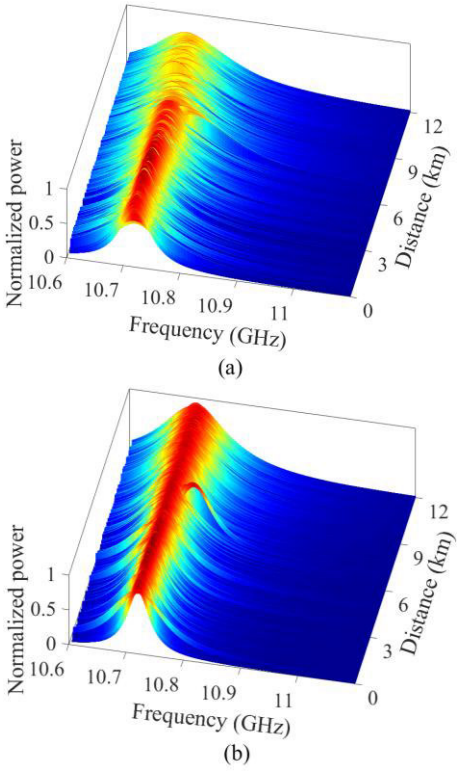

FIGURE 5. Results of Lorentzian-curve fitting. (a) full fitting and (b) half-peak fitting.

amplifier (EDFA) and filtered by fiber Bragg grating (FBG) and demodulated coherently through a coupler and detected by photodetector (PD) as the Brillouin reflection signal. The Brillouin reflection signal was amplified by an intermediate frequency amplifier (IFA) and heterodyne detected with an RF signal of 10.624 GHz generated by microwave generator (MG). A low-frequency signal of approximately 100 MHz was obtained and amplified again by low frequency amplifier (LFA). Finally, a 1 G/Sample data acquisition card (DAQ) was used to capture the signal for data processing.

By performing STFT with the Brillouin signal data collected in the experiment, the power spectra were obtained and cumulatively averaged 200 times to analyze the effects of Lorentzian-curve fitting. The curves obtained by full fitting are shown in Fig. 6(a). With an increase in the distance, the stability of the curve peak worsens, and some curves clearly deform. The curves obtained by half-peak fitting are shown in Fig. 6(b). The curve peak is steady, and the BFS in the temperature-change section is clear at 7 km.

As shown in Fig. 7(a), there are many large jitters in the BFS profile obtained by full fitting. The errors of BFSs obviously increase with distance, and some errors even exceed 10 MHz. As shown in Fig. 7(b), the jitters are smaller in the BFS profile obtained by half-peak fitting. BFSs stabilize at 10.72 GHz, and their errors are almost less than 3 MHz. After calculation, the measurement accuracy of BFS in full fitting is 3.76 MHz, and it is 1.56 MHz in half-peak fitting. As BFS is linearly related to both temperature and strain, the corresponding temperature

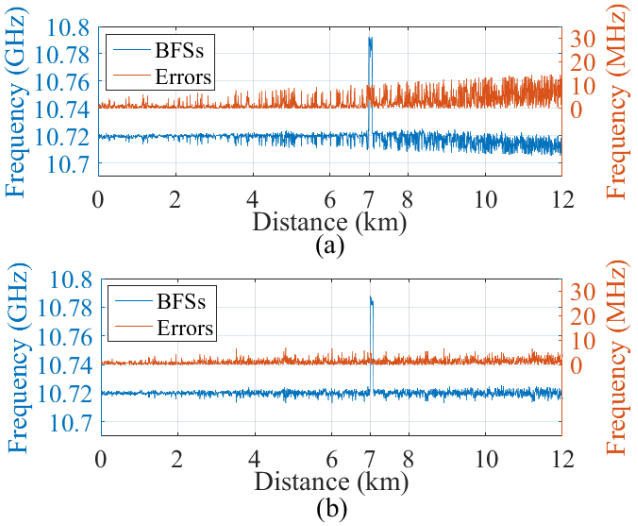

FIGURE 6. Comparison of BFS profiles. (a) full fitting and (b) half-peak fitting.

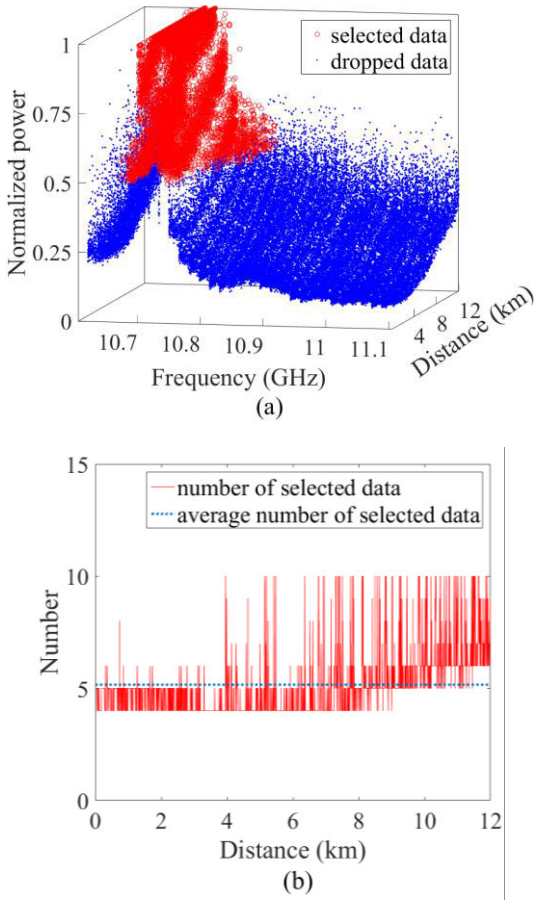

FIGURE 7. (a) Result of half-peak selecting and (b)Quantity statistics of selected data.

measurement accuracy is changed from 3.2°C to 1.3°C, and the corresponding strain measurement accuracy is changed from 75.2 $\mu\varepsilon$ to 31.2 $\mu\varepsilon$. Therefore, the half-peak algorithm can reduce the error by more than half and effectively improve the accuracy and stability of BFS measurements.

TABLE 1. Measurement accuracy by various fitting algorithms.

Algorithms	Measurement accuracy		
	BFS (MHz)	Temperature (°C)	Strain (με)
Lewenberg–Marquardt	2.47	2.1	49.4
PSO-LCF [13]	2.38	2.0	47.6
ANN-model [14]	2.88	2.4	57.6
least-squares full fitting	3.76	3.2	75.2
half-peak fitting	1.56	1.3	31.2

Because only a small portion of the data from the upper half of the main peak were selected for least-squares fitting, the calculation was significantly reduced. The power spectrum data at each position of the FUT in the experiment are shown in Fig. 8(a), where the red points represent the data selected for fitting. The number of half-peak data points is reduced to the range of 4-10, as shown in Fig. 8(b), and the average number is 5.16. Compared with the number of 32 used in full fitting, the calculation of the half-peak algorithm is reduced by ∼80%. Therefore, the proposed algorithm effectively reduces the computational complexity, saves considerable computing time, and significantly improves real-time performance.

In the experiment, the STFT of single-step sliding was used to obtain the details of the power spectra in the temperature-change section, where the profile of each power spectrum is a double-peak curve because the Brillouin backscatter signals before and after the temperature change are all contained in the sliding window. As the window slides, the proportion of signals after the temperature change increases and the corresponding peak value increases, as shown in Fig. 8(a). The power spectra, which were fully fitted by a Lorentzian-curve, are shown in Fig. 8(b). Because the double-peak data cannot be strictly fitted by the Lorentzian-curve, the peak of the full fitting lies between the two peaks of the power spectrum. The BFS gradually changes along the FUT in the temperature-change section, as shown in Fig. 8(c). The half-peak data are indicated by red points in Fig. 8(d). The power spectra obtained via half-peak fitting are shown in Fig. 8(e). The BFS jumps from one peak to another at the edge of the temperature change, which accurately reflects the spatial location of the event, as shown in Fig. 8(f). The relationship between spatial resolution and sampling rate is expressed as Eq. (4):

$$\Delta z = \frac{c}{2nF_S} \tag{4}$$

where Δz is spatial resolution, F_S is sampling rate, c is light speed, n is refractive index of fiber. In the experiment, the sampling rate is 1 GHz and n is 1.5, the spatial resolution has a theorical value 0.1 m. If the change of BFS is detected by single-step, the spatial resolution of the temperature change position just is 0.1 m and reaches the maximum limitation with this sampling rate. Therefore, this algorithm can eliminate the influence of the minor peak and determine the position of an event with a high spatial resolution.

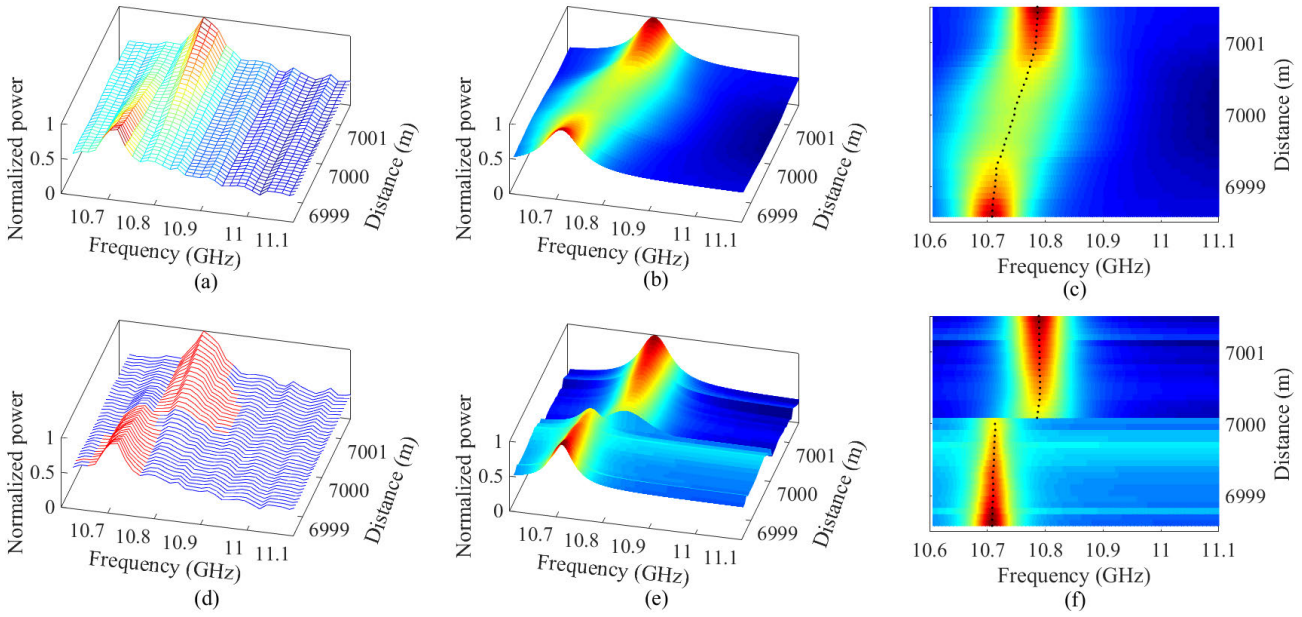

FIGURE 8. Fitting effect of double-peak spectrum by two algorithms. (a) the data of double-peak spectrum, (b) full fitted by Lorentzian-curve, (c) BFSs of full fitting, (d) result of half-peak selecting, (e) half-peak fitted by Lorentzian-curve, and (f) BFSs of half-peak fitting.

IV. CONCLUSION

We propose a half-peak fitting algorithm to precisely measure the BFS in the BOTDR. In the verification experiment, a probe light with 50 ns width was injected into the 12 km FUT. After coherent demodulation and heterodyne detection, low-frequency signals of ∼100 MHz were acquired at a sampling rate of 1 GHz, and the data of the Brillouin power spectrum were obtained by STFT and cumulatively averaged 200 times. The experimental results show that the measurement accuracy of BFS is reduced from 3.76 MHz to 1.56 MHz by the half-peak fitting method, which improves the measurement accuracy by ∼100% and significantly enhances the stability. Simultaneously, this algorithm can effectively shield the interference of the minor peak data and the spatial resolution of the edge of BFS jumping; that is, the temperature change position can reach 0.1 m, which is the maximum limit of the sampling rate. Moreover, this algorithm is intuitive, easy to implement with a small amount of computation, reduces the fitting calculation by approximately 80%, significantly increases measurement speed, and is highly practical.

REFERENCES

[1] T. Kurashima, T. Horiguchi, H. Izumita, S. I. Furukawa, and Y. Koyamada, "Brillouin optical-fiber time domain reflectometry," *IEICE Trans. Commun.*, vol. 76, pp. 382–390, Apr. 1993.

[2] Q. Bai, Q. Wang, D. Wang, Y. Wang, Y. Gao, H. Zhang, M. Zhang, and B. Jin, "Recent advances in Brillouin optical time domain reflectometry," *Sensors*, vol. 19, no. 8, p. 1862, Apr. 2019, doi: 10.3390/s19081862.

[3] H. Zhang, D. Zhou, B. Wang, C. Pang, P. Xu, T. Jiang, D. Ba, H. Li, and Y. Dong, "Recent progress in fast distributed Brillouin optical fiber sensing," *Appl. Sci.*, vol. 8, no. 10, p. 1820, Oct. 2018, doi: 10.3390/app8101820.

[4] L. Luo, Y. Mei, N. Battista, C. Kechavarzi, and K. Soga, "Repeatability precision error analysis of the distributed fiber optic strain monitoring," *Struct. Control Health Monitor.*, vol. 28, no. 8, p. e2768, Aug. 2021, doi: 10.1002/stc.2768.

[5] T. Sasaki, S. H. Zhang, K. Soga, L. Q. Luo, B. Freifeld, Y. Kitayama, K. Kawaguchi, and H. Sugiyama, "Distributed fiber optic strain sensing of bending deformation of a well mockup in the laboratory," *J. Natural Gas Sci. Eng.*, vol. 96, Dec. 2021, Art. no. 104309, doi: 10.1016/j.jngse.2021.104309.

[6] R. Min, Z. Liu, L. Pereira, C. Yang, Q. Sui, and C. Marques, "Optical fiber sensing for marine environment and marine structural health monitoring: A review," *Opt. Laser Technol.*, vol. 140, Aug. 2021, Art. no. 107082, doi: 10.1016/j.optlastec.2021.107082.

[7] G. T. Webb, P. J. Vardanega, N. A. Hoult, P. Fidler, P. J. Bennett, and C. R. Middleton, "Analysis of fiber-optic strain-monitoring data from a prestressed concrete bridge," *J. Bridge Eng.*, vol. 22, no. 5, 2017, Art. no. 05017002, doi: 10.1061/(ASCE)BE.1943-5592.0000996.

[8] L. Luo, H. Sekiya, and K. Soga, "Dynamic distributed fiber optic strain sensing on movement detection," *IEEE Sensors J.*, vol. 19, no. 14, pp. 5639–5644, Jul. 2019, doi: 10.1109/JSEN.2019.2907889.

[9] G. J. Tu, X. P. Zhang, Y. X. Zhang, Z. F. Ying, and L. D. Lv, "Strain variation measurement with short-time Fourier transform-based Brillouin optical time-domain reflectometry sensing system," *Electron. Lett.*, vol. 50, no. 22, pp. 1624–1625, 2014, doi: 10.1049/el.2014.2470.

[10] W. Li, L. Jiang, T. Zhang, L. Cheng, H. Liang, L. Zhou, W. Liu, L. Shao, and B.-O. Guan, "Brillouin frequency estimation in distributed Brillouin optical fiber sensors based on instantaneous frequency," *IEEE Sensors J.*, vol. 22, no. 19, pp. 18501–18507, Oct. 2022, doi: 10.1109/JSEN.2022.3200989.

[11] Y. Zhang, D. Li, X. Fu, and W. Bi, "An improved Levenberg–Marquardt algorithm for extracting the features of Brillouin scattering spectrum," *Meas. Sci. Technol.*, vol. 24, no. 1, Jan. 2013, Art. no. 015204, doi: 10.1088/0957-0233/24/1/015204.

[12] Y. Zhang, Y. Zhao, X. Fu, and J. Xu, "A feature extraction method of the particle swarm optimization algorithm based on adaptive inertia weight and chaos optimization for Brillouin scattering spectra," *Opt. Commun.*, vol. 376, pp. 56–66, Oct. 2016, doi: 10.1016/j.optcom.2016.04.049.

[13] X. Li, L. Xi, Y. Zhang, X. Yuan, and X. Zhang, "Application of the joint algorithm of smooth pseudo Wigner–Ville distribution and four-parameter particle swarm optimization to BOTDR," *Results Phys.*, vol. 25, Jun. 2021, Art. no. 104215, doi: 10.1016/j.rinp.2021.104215.

[14] A. S. K. Almoosa, A. E. Hamzah, M. S. D. Zan, M. F. Ibrahim, N. Arsad, and M. M. Elgaud, "Improving the Brillouin frequency shift measurement resolution in the Brillouin optical time domain reflectometry (BOTDR) fiber sensor by artificial neural network (ANN)," *Opt. Fiber Technol.*, vol. 70, May 2022, Art. no. 102860, doi: 10.1016/j.yofte.2022.102860.

[15] B. Chen, L. Su, Z. Zhang, X. Liu, M. Song, H. Yu, Y. Wang, and J. Yang, "Wavelet convolutional neural network for robust and fast temperature measurements in Brillouin optical time domain reflectometry," *Opt. Exp.*, vol. 30, no. 9, pp. 13942–13958, 2022, doi: 10.1364/OE.451877.
[16] D. Sanogo, Y. Pan, P. Xu, D. Zhou, B. Wang, L. Teng, Z. Lu, D. Ba, and Y. Dong, "Detecting cm-scale hot spot over 24-km-long single-mode fiber by using differential pulse pair BOTDA based on double-peak spectrum," *Opt. Exp.*, vol. 25, no. 15, pp. 17727–17736, 2017, doi: 10.1364/OE.25.017727.
[17] Y. Yu, L. Luo, B. Li, L. Guo, J. Yan, and K. Soga, "Double peak-induced distance error in short-time-Fourier-transform-Brillouin optical time domain reflectometers event detection and the recovery method," *Appl. Opt.*, vol. 54, no. 28, p. E196, Oct. 2015, doi: 10.1364/AO.54.00E196.
[18] Q. He, H. Jiang, Z. Wang, S. Ye, X. Shang, T. Li, and L. Tang, "Spatial resolution enhancement of DFT-BOTDR with high-order self-convolution window," *Opt. Fiber Technol.*, vol. 57, Jul. 2020, Art. no. 102188, doi: 10.1016/j.yofte.2020.102188.
[19] Y. Zhang, P. Jin, X. Fu, F. Zhang, J. Hou, and J. Xu, "Feature extraction of multi-peak Brillouin scattering spectrum based on SFLA-LSSVM algorithm," *Chin. J. Lasers*, vol. 45, no. 1, 2018, Art. no. 0106004, doi: 10.3788/CJL201845.0106004.
[20] M. Niklès, L. Thévenaz, and P. A. Robert, "Brillouin gain spectrum characterization in single-mode optical fibers," *J. Lightw. Technol.*, vol. 15, no. 10, pp. 1842–1851, Oct. 1997, doi: 10.1109/50.633570.

DONG WAN received the B.S. degree in communication engineering from Jilin University, China, in 2002. He is currently pursuing the Ph.D. degree in electronic science and technology with the Beijing University of Posts and Telecommunications, Beijing, China. He is also an Associate Professor with the Beijing Information and Technology College, Beijing. His research interests include optical fiber sensors, optical communication, and electronic information engineering technology.

LINAN SHAN is currently pursuing the Ph.D. degree in electronic science and technology with the Beijing University of Posts and Telecommunications, Beijing, China. Her research interests include optical fiber sensors and polarization effects in optical fibers.

LIXIA XI received the B.S. degree in physics from Hebei Normal University, Hebei, China, in 1994, the M.S. degree in physics from Beijing Normal University, Beijing, China, in 1997, and the Ph.D. degree in physical electronics from the Beijing University of Posts and Telecommunications, Beijing, in 2005. She is currently a Professor with the Beijing University of Posts and Telecommunications. Her research interests include high-speed optical fiber communication and optical sensors.

ZHENYU XIAO is currently pursuing the Ph.D. degree in information and communication engineering with the Beijing University of Posts and Telecommunications, Beijing, China. His research interests include optical fiber sensors and signal processing.

YANG'AN ZHANG received the degree from the Beijing University of Posts and Telecommunications, in 2001. He has been an Associate Professor with the Beijing University of Posts and Telecommunications. His research interests include the application of embedded signal processing technology in high-speed optical communication and optical sensing.

XUEGUANG YUAN received the Ph.D. degree in electromagnetic fields and microwave technology from the Beijing University of Posts and Telecommunications, in 2009. He was a Postdoctoral Researcher with the State Key Laboratory of Information Photonics and Optical Communications, from 2009 to 2011, where he is currently an Associate Professor. His research interests include optical communication and photoelectric sensing.

XIAOSHENG XIAO (Senior Member, IEEE) received the B.E. and Ph.D. degrees from Tsinghua University, Beijing, China, in 2002 and 2007, respectively. From 2007 to 2008, he was with the Network Technology Research Centre, Nanyang Technological University, Singapore, as a Research Fellow. From 2009 to 2019, he was an Assistant Professor and an Associate Professor with the Department of Precision Instruments, Tsinghua University. Since 2019, he has been an Associate Professor with the State Key Laboratory of Information Photonics and Optical Communications, Beijing University of Posts and Telecommunications, Beijing. His research interests include mode-locked fiber lasers, optical fiber communications, and fiber optics.

HU ZHANG received the Ph.D. degree in electromagnetic field and microwave technology from the Beijing University of Posts and Telecommunications, Beijing, China, in 2009. He is currently an Associate Professor with the School of Electric Engineering, Beijing University of Posts and Telecommunications. He has coauthored more than 70 peer-reviewed journals and conference papers. His research interests include special optical fiber, fiber devices, and space division multiplexing technology.

XIAOGUANG ZHANG (Senior Member, IEEE) received the B.S. and M.S. degrees in physics from Peking University, Beijing, China, in 1985 and 1988, respectively, and the Ph.D. degree in physical electronics from the Beijing University of Posts and Telecommunications, Beijing, in 2004. He is currently a Professor with the Institute of Information Photonics and Optical Communications, Beijing University of Posts and Telecommunications. His research interests include polarization effects in fibers and high-speed optical communication systems. He is a member of OSA and a Senior Member of the Chinese Optics Society. He is also a Syndic of the Beijing Optics Society (BOS) and the Chair of the Committee of Optical Communications, BOS.